

# FERMI AND NON-FERMI LIQUID BEHAVIOR OF LOCAL MOMENT SYSTEMS WITHIN A CONSERVING SLAVE BOSON THEORY

JOHANN KROHA and PETER WÖLFLE

*Institut für Theorie der Kondensierten Materie, Universität Karlsruhe, Postfach  
6980, 76128 Karlsruhe, Germany*

The question of Fermi liquid vs. non-Fermi liquid behavior induced by strong correlations is one of the prominent problems in metallic local moment systems. As standard models for such systems, the  $SU(N) \times SU(M)$  Anderson impurity models exhibit both Fermi liquid and non-Fermi liquid behavior, depending on their symmetry. Using an auxiliary boson method, we present a generally applicable scheme to select the relevant contributions in the low frequency regime, while preserving the local gauge symmetry of the model. It amounts to a conserving T-matrix approximation (CTMA) including coherent spin flip as well as charge fluctuation processes, which are found to dominate in the Kondo and in the mixed valence regime, respectively. The infrared threshold exponents of the auxiliary particle spectral functions are indicators for the presence of Fermi or non-Fermi liquid behavior in any given model with strong on-site repulsion. We show that, in contrast to earlier auxiliary boson theories, the CTMA recovers the correct exponents in both cases, indicating that it correctly describes both the Fermi and the non-Fermi regimes of the Anderson model.

## 1 Introduction

It is a remarkable feature of interacting, itinerant fermion systems that at low temperatures  $T$  they behave in general in much the same way as a noninteracting Fermi gas, even though the interaction may be strong. An extremely successful description of this phenomenon, known as Fermi liquid (FL) behavior, is provided by the notion of quasiparticles, which was established by Landau's phenomenological Fermi liquid theory<sup>1</sup>. The key assumption is that, as the interaction is continuously turned on, there exists a 1:1 correspondence between the low energy eigenstates of the interacting system and the single-particle states of the free Fermi gas. Therefore, the low-lying interacting states may be described approximately as single-particle states or quasiparticles, whose decay rate  $1/\tau$  is small compared to their excitation energy  $\omega$ ,  $1/\tau \ll \omega$ , and which are characterized by the same quantum numbers as the noninteracting states. As a consequence, Fermi liquids exhibit the same low- $T$  thermodynamics as a noninteracting Fermi system, e.g. a linear in  $T$  specific heat  $c = \gamma T$  and a constant Pauli paramagnetic susceptibility  $\chi_0$ . However, the effective mass and other parameters may be renormalized by the interaction, resulting in an enhancement of the specific heat coefficient  $\gamma$  and the susceptibility  $\chi_0$ .

It is at the heart of the quasiparticle picture that at low  $T$  the Pauli exclusion principle substantially reduces the phase space available to quasiparticle scattering. This blocking mechanism is effective as long as the quasiparticle interaction is *shortranged in space and time*, which is usually the case in three dimensions because of screening. It also implies that the quasiparticle scattering rate vanishes as  $1/\tau \propto (\omega^2 + T^2)$ , thus providing a microscopic justification for the basic assumption of FL theory and leading to an interaction contribution to the electrical resistivity which behaves as  $\Delta\rho \propto T^2$ . Obviously, the Pauli principle as the origin of FL behavior is very robust, which explains the almost ubiquitous presence of a FL ground state in interacting Fermi systems and the broad success of Fermi liquid theory.

In this light it is all the more exciting that in recent years a number of new alloys have been discovered which exhibit striking deviations from this usual behavior. Among these, an important subclass are certain heavy fermion compounds on the basis of  $\text{Ce}^{3+}$  or  $\text{U}^{4+}$  ions, e.g.  $\text{CeCu}_{6-x}\text{Au}_x$ <sup>2,3</sup>,  $\text{CeCu}_2\text{Si}_2$ <sup>4</sup>,  $\text{CePd}_2\text{Si}_2$ <sup>5,6</sup> and  $\text{Y}_{1-x}\text{U}_x\text{Pd}_3$ <sup>7</sup> or  $\text{UCu}_{5-x}\text{Pt}_x$ <sup>8</sup>. In these materials logarithmic or fractional power law deviations from FL behavior have been observed in their thermodynamic as well as transport properties at low temperatures. These systems have in common that a localized, degenerate degree of freedom, the magnetic moments of the Ce or U ions, is dynamically coupled to a continuum of conduction electron states. In general, such a coupling generates the Kondo effect, characterized by resonant spin flip scattering of electrons at the Fermi surface off the local moment. Concomitantly, the conduction electron spin flip rate initially increases logarithmically as the temperature is lowered, passes through a maximum at a characteristic scale, the Kondo temperature  $T_K$ , and approaches zero as  $T \rightarrow 0$ , because the effective local moment becomes screened by the conduction electron spins. Thus, even for many strongly correlated systems of this type a Fermi liquid description applies below  $T_K$ , with usually a strongly enhanced quasiparticle effective mass, lending the term “heavy fermion systems” to these materials.

Completely new physics may arise, however, if the quenching of the local moments is inhibited. Two different mechanisms for this to occur have been put forward:

- (1) Proximity of a quantum phase transition (QPT) to an antiferromagnetically ordered state<sup>9-12</sup> as a function of a dopant concentration  $x$  or of pressure. Near the QPT the quantum critical fluctuations become longranged in space and time and can, thus, mediate a longrange quasiparticle interaction, leading to a breakdown of FL theory. There are indications for this spatially extended mechanism to be realized near the QPT of the Ce based compounds<sup>2-6</sup>.

- (2) Two-channel Kondo effect (2CK)<sup>13,14</sup>. The local magnetic moment is coupled to two exactly degenerate conduction electron channels. Because of a frustration effect between the screening of the local moment by the different conduction channels the moment quenching cannot be complete, leading to a nonvanishing conduction electron spin scattering rate even at the lowest temperatures and subsequently to a breakdown of FL behavior. It has been suggested<sup>15</sup> that this mechanism, based on single-ion dynamics rather than longrange fluctuations, may be realized predominantly in the U based materials with cubic symmetry about the magnetic ion, which do not exhibit a QPT.

While both mechanisms provide possible pathways to non-FL behavior, neither one can at present consistently explain the wealth of experimental data showing non-FL behavior at low temperatures. Open questions in the QPT picture include, e.g., whether the local impurity dynamics competing with the magnetic ordering can play a role, and how the transition from the spin screened heavy FL phase to the magnetically ordered phase occurs altogether. In the 2CK mechanism, on the other hand, inter-impurity interactions could modify the single ion behavior. Exact solution methods as well as numerical simulations have provided important progress in our understanding of strongly correlated quantum impurity systems. However, their applicability is essentially restricted to problems involving only a single impurity, owing to integrability conditions or limitations in the numerical effort, respectively. Therefore, more generally applicable theoretical techniques are called for. In the present work we focus on the single-ion dynamics. We develop a standard field theoretical method, based on an auxiliary particle or slave boson representation, which describes the quantum impurity dynamics in a controlled way and at the same time has the potential of being extended to problems of many impurities on a lattice. As a standard model of strongly correlated electrons which, depending on its symmetry, exhibits both FL and non-FL behavior, we consider the  $SU(N)\times SU(M)$  Anderson impurity model of a local,  $N$ -fold degenerate degree of freedom, coupled to  $M$  identical conduction bands.

In order to set the stage for the more formal development of the theory, in the following section we will briefly review the striking differences in the phenomenology of the single-channel and the multi-channel Kondo effects. In section 3 the slave boson representation is introduced, which provides a particularly compact formulation of the  $SU(N)\times SU(M)$  Anderson model. We also discuss why the presence of FL or non-FL behavior in a given quantum impurity system can already be seen from the singular infrared dynamics of the auxiliary particles. Section 4 contains a critical assessment of earlier approximate slave boson treatments. This will motivate our approach of conserving

slave boson approximations, which is developed in section 5. As will be seen, the results produced from this theory are in very good agreement with known exact properties of the model. Conclusions are drawn in section 6.

## 2 Single- and multi-channel Kondo effect and physical realizations

In this section we briefly discuss how the single-channel and the two-channel Kondo effects may arise in magnetic metals, if the interaction between the local moments is weak. A local moment is generated by an atomic f or d level whose energy  $E_d$  lies far below the Fermi energy  $\varepsilon_F \equiv 0$  and whose electron occupation number is effectively restricted to  $n_d \leq 1$  by a strong Coulomb repulsion  $U$  between two electrons in the same orbital. While the angular momentum degeneracy of the level is usually lifted by crystal field splitting, a twofold degeneracy of a level occupied by one electron is guaranteed by time reversal symmetry (Kramers doublet) in the absence of a magnetic field, corresponding to the spin quantum numbers  $m = \pm 1/2$  of the electron. In addition, there is a hybridization matrix element  $V$  between the atomic orbital and the conduction electron states. Such a system is described by the single impurity Anderson hamiltonian

$$H = \sum_{\vec{k},\sigma} \varepsilon_{\vec{k}} c_{\vec{k}\sigma}^\dagger c_{\vec{k}\sigma} + E_d \sum_{\sigma} d_{\sigma}^\dagger d_{\sigma} + V \sum_{\vec{k},\sigma} (c_{\vec{k}\sigma}^\dagger d_{\sigma} + h.c.) + U d_{\uparrow}^\dagger d_{\uparrow} d_{\downarrow}^\dagger d_{\downarrow}, \quad (1)$$

where  $c_{\vec{k}\sigma}^\dagger$  and  $d_{\sigma}^\dagger$  are the creation operators of a conduction electron with dispersion  $\varepsilon_{\vec{k}}$  and of an electron in the local orbital with spin  $\sigma$ , respectively. The low energy physics of this system is dominated by processes of second order in  $V$ , by which an electron hybridizes into the conduction band and the impurity level is subsequently filled by another electron, thereby effectively flipping the impurity spin. Thus, in the region of low excitation energies, the Anderson hamiltonian (1) may be mapped onto the s-d exchange (or Kondo) model<sup>16</sup>, the effective coupling between the impurity spin and the conduction electron spin always being antiferromagnetic:  $J = |V|^2/|E_d| > 0$  ( $U \gg |E_d|$ ). These models have been studied extensively by means of Wilson's renormalization group<sup>17</sup> and by the Bethe ansatz method<sup>18</sup>. In this way the following physical picture has emerged. Resonant spin flip scattering of electrons at the Fermi surface off the local degenerate level leads to logarithmic contributions to the magnetic susceptibility, the linear specific heat coefficient and the resistivity,  $\chi(T)$ ,  $\gamma(T)$ ,  $\Delta\rho(T) \propto \ln(T/T_K)$ , for  $T \gtrsim T_K$ , and to a breakdown of perturbation theory at the Kondo temperature  $T_K = D(N\mathcal{N}(0)J)^{(M/N)} \exp\{-1/(N\mathcal{N}(0)J)\}$ . Here  $\mathcal{N}(0)$  and  $D$  denote

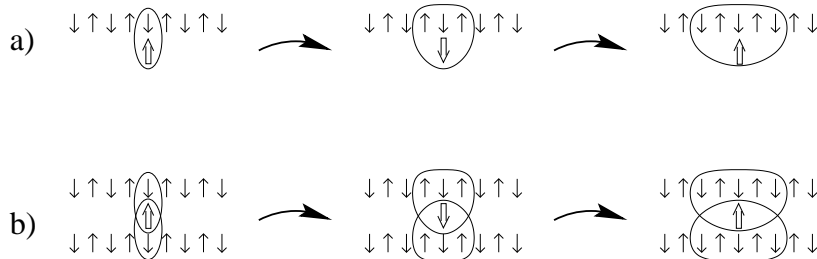


Figure 1: Sketch of the renormalization group for a) the single-channel Kondo model (local moment compensation) and b) the two-channel Kondo model (local moment over-compensation). Small arrows denote conduction electron spins  $1/2$ , a heavy arrow a localized spin  $1/2$ . The curved arrows indicate successive renormalization steps.

the density of states at the Fermi energy and the high energy band cutoff, respectively, and  $N$ ,  $M$  are the degeneracy of the local level and the number of conduction electron channels (see below). Below  $T_K$  a collective many-body spin singlet state develops in which the impurity spin is screened by the conduction electron spins as lower and lower energy scales are successively approached, leaving the system with a pure potential scattering center. The spin singlet formation is sketched in Fig. 1 a) and corresponds to a vanishing entropy at  $T = 0$ ,  $S(0) = 0$ . It also leads to saturated behavior of physical quantities below  $T_K$ , like  $\chi(T) = const$ ,  $c(T)/T = const$ . and  $\Delta\rho(T) \propto T^2$ , i.e. to Fermi liquid behavior.

As an example of possible two-channel Kondo systems we discuss the uranium based compounds mentioned in the introduction. The  $U^{4+}$  ions have nominally a  $5f^2$  configuration, i.e. an even number of electrons, which does not allow for a Kramers degenerate ground state because of integer total spin. However, in the cubic crystal symmetry of these materials the orbital degeneracy may be not completely lifted, so that there can be an approximate twofold degeneracy of the  $U^{4+}$  ground state, corresponding to two different orientations of the electrical quadrupole moment of the  $5f$  orbital in the lattice (quadrupolar Kondo effect)<sup>14,15</sup>. This degree of freedom may be flipped by scattering of conduction electrons (which in the cubic symmetry also have a twofold angular momentum degeneracy). The conduction electron spin is conserved in this scattering process, leaving it as a Kramers degenerate scattering channel degree of freedom, which we will label by  $\mu = 1, \dots, M$ ,  $M = 2$ . Describing the orbital degree of freedom as a pseudospin  $1/2$ , labelled by the quantum number  $\sigma = 1, \dots, N$ ,  $N = 2$ , in analogy to the magnetic Kondo effect, we

arrive at the  $SU(2)\times SU(M)$  symmetric Kondo model,

$$H = \sum_{\vec{k},\sigma,\mu} \varepsilon_{\vec{k}} c_{\vec{k}\sigma}^\dagger c_{\vec{k}\mu\sigma} + J \sum_{\vec{k},\vec{k}',\sigma,\sigma',\mu} c_{\vec{k}\mu\sigma}^\dagger \vec{S} \cdot \vec{\tau}_{\sigma\sigma'} c_{\vec{k}'\mu\sigma'}, \quad (2)$$

where  $\vec{S}$  is the local pseudospin operator and  $\vec{\tau}_{\sigma\sigma'}$  the vector of Pauli matrices. To keep the naming uniform, we will refer to the orbital degree of freedom as the (pseudo)spin or local moment,  $\sigma$ , in analogy to the magnetic Kondo effect, and to the physical electron spin as the channel degree of freedom,  $\mu$ . In the multi-channel case, too, the conduction electrons of each channel *separately* screen the impurity moment by multiple spin scattering at temperatures below the Kondo scale  $T_K$ . However, in this case, the local moment is over-compensated, since the impurity spin can never form a singlet state with both conduction electron channels at the same time in this way, as can be seen in Fig. 1 b). As a consequence of this frustration, there is not a unique ground state, leading to a finite residual entropy<sup>19</sup> at  $T = 0$  of  $S(0) = k_B \ln\sqrt{2}$  in the two-channel model. In particular, the precondition of FL theory of a 1:1 correspondence between interacting and non-interacting states is violated. As a consequence, characteristic singular temperature dependence<sup>20,21</sup> of physical quantities persists for  $T \lesssim T_K$  down to  $T = 0$ :  $\chi(T) \propto -\ln(T/T_K)$ ,  $c(T)/T \propto -\ln(T/T_K)$  and  $\rho(T) - \rho(0) \propto -\sqrt{T/T_K}$ . Note, however, that this behavior may be changed by any crystal field splitting of the quadrupolar non-Kramers ground state doublet.

In order to apply standard field theoretical methods to the multi-channel Kondo model it is convenient to consider it as the low-energy limiting case of a corresponding Anderson model as discussed for the single-channel case. Here, in addition, the conservation of the channel degree of freedom has to be guaranteed. This can be implemented in an elegant way using an auxiliary boson representation to be discussed in the next section.

### 3 Auxiliary particle representation

As discussed above, the local level of a quantum impurity in the limit of infinitely strong local Coulomb repulsion  $U$  between electrons in the same level allows only for at most single electron occupation of the level,  $n_d \leq 1$ . One should note that for a realistic finite value of  $U$  the low-energy physics of the model is effectively still confined to the part of the Hilbert space without multiple occupancy. Therefore, the model Eq. (1) in the limit  $U \rightarrow \infty$  is the generic model for the physics of quantum impurities at large  $U$  in general.

A powerful technique for implementing the projection in Hilbert space caused by a large Coulomb repulsion  $U$  is the method of auxiliary particles

(slave bosons, pseudofermions)<sup>22</sup>. Each Fock state  $|\alpha\rangle$  of the impurity is assigned a creation operator, which can be envisaged as creating the state out of a vacuum state  $|\text{vac}\rangle$  without any impurity level at all,  $|\alpha\rangle = a_\alpha^\dagger |\text{vac}\rangle$ . (E.g., for a single orbital there are four such states,  $|0\rangle$  (empty orbital),  $|\uparrow\rangle$  or  $|\downarrow\rangle$  (orbital occupied by a single electron with spin  $\uparrow$  or  $\downarrow$ ) and  $|2\rangle$  (level occupied by two electrons with spin  $\uparrow$  and  $\downarrow$ )). Due to the requirements of Fermi statistics, the creation operators  $a_\alpha^\dagger$  are Fermi (Bose) operators for the states holding an odd (even) number of electrons (or vice versa). The physical state corresponds to the sector of Fock space with exactly one auxiliary particle,  $\sum_\alpha n_\alpha = 1$ , where  $n_\alpha = a_\alpha^\dagger a_\alpha$  is the occupation number operator of particles  $\alpha$ . Compared to alternative ways of effecting the projection, the auxiliary particle method has the advantage of making available the powerful machinery of quantum field theory, provided the constraint on the total auxiliary particle number can be incorporated in a satisfactory way.

For the quantum impurity models of the Anderson type introduced in the preceding section, only particles creating empty and singly occupied states are needed. We define  $N$  pseudofermion creation operators  $f_\sigma^\dagger$  for each of the singly occupied states (labelled by  $\sigma = 1, 2, \dots, N$ ) and  $M$  boson creation operators  $b_\mu^\dagger$  for each of the empty states created when an electron hops from the impurity into the  $\mu$ -th conduction electron band (labelled by  $\mu = 1, 2, \dots, M$ ). In terms of these operators the Hamiltonian of the  $SU(N) \times SU(M)$  Anderson model Eq. (1) takes the form

$$H = \sum_{\vec{k}, \sigma, \mu} \varepsilon_{\vec{k}} c_{\vec{k}\mu\sigma}^\dagger c_{\vec{k}\mu\sigma} + E_d \sum_{\sigma} f_\sigma^\dagger f_\sigma + V \sum_{\vec{k}, \sigma, \mu} (c_{\vec{k}\mu\sigma}^\dagger b_\mu^\dagger f_\sigma + h.c.) \quad (3)$$

In addition, the operator constraint

$$Q \equiv \sum_{\sigma} f_\sigma^\dagger f_\sigma + \sum_{\mu} b_\mu^\dagger b_\mu = 1 \quad (4)$$

has to be satisfied at all times. One might interpret the constraint as a statement of charge quantization, with the integer  $Q$  the conserved, quantized charge. Similar to quantum field theories with conserved charges, the charge conservation is intimately related to the existence of a local gauge symmetry. Indeed, the system defined by the Hamiltonian Eq. (3) is invariant under simultaneous local  $U(1)$  gauge transformations  $f_\sigma \rightarrow f_\sigma e^{i\phi(\tau)}$ ,  $b_\mu \rightarrow b_\mu e^{i\phi(\tau)}$ , with  $\phi(\tau)$  an arbitrary time dependent phase.

While the gauge symmetry guarantees the conservation of the quantized charge  $Q$ , it does not single out any particular  $Q$ , such as  $Q = 1$ . In order to effect the projection onto the sector of Fock space with  $Q = 1$ , one may use

a procedure first proposed by Abrikosov<sup>23</sup>: Consider first the grand canonical ensemble with respect to  $Q$ , defined by the statistical operator

$$\hat{\rho}_G = \frac{1}{Z_G} e^{-\beta(H + \lambda Q)}, \quad (5)$$

where  $Z_G = \text{tr}[\exp(-\beta(H + \lambda Q))]$  is the grand canonical partition function and the trace extends over the complete Fock space, including summation over  $Q$ . The expectation value of an observable  $A$  in the grand canonical ensemble is given by

$$\langle A \rangle_G = \text{tr}[\hat{\rho}_G A]. \quad (6)$$

The physical expectation value of  $A$ ,  $\langle A \rangle$ , is to be evaluated in the canonical ensemble where  $Q = 1$ . It can be calculated from the grand canonical ensemble by taking the chemical potential  $\lambda$  to infinity,

$$\langle A \rangle = \lim_{\lambda \rightarrow \infty} \frac{\langle QA \rangle_G}{\langle Q \rangle_G}. \quad (7)$$

In the following we will concentrate on the auxiliary particle Green's functions in the grand canonical ensemble as the basic building blocks of the theory. In imaginary time representation they are defined as

$$\begin{aligned} G_{f\sigma}(\tau_1 - \tau_2) &= -\langle T \{ f_\sigma(\tau_1) f_\sigma^\dagger(\tau_2) \} \rangle_G \\ G_{b\mu}(\tau_1 - \tau_2) &= -\langle T \{ b_\mu(\tau_1) b_\mu^\dagger(\tau_2) \} \rangle_G, \end{aligned} \quad (8)$$

where  $T$  is the time ordering operator. The Fourier transforms of  $G_{f,b}$  and of the local conduction electron Green's function may be expressed in terms of the self-energies  $\Sigma_{f,b,c}$  as

$$G_{f,b,c}(i\omega_n) = \left\{ [G_{f,b,c}^0(i\omega_n)]^{-1} - \Sigma_{f,b,c}(i\omega_n) \right\}^{-1} \quad (9)$$

where

$$\begin{aligned} G_{f\sigma}^0(i\omega_n) &= (i\omega_n - E_d - \lambda)^{-1} \\ G_{b\mu}^0(i\omega_n) &= (i\omega_n - \lambda)^{-1} \\ G_{c\mu\sigma}^0(i\omega_n) &= \sum_{\vec{k}} (i\omega_n - \epsilon_{\vec{k}})^{-1} \end{aligned} \quad (10)$$

The Green's functions  $G_{f,b,c}$  have the following spectral representations

$$G_{f,b,c}(i\omega_n) = \int_{-\infty}^{\infty} \frac{d\omega'}{\pi} \frac{A_{f,b,c}(\omega')}{i\omega_n - \omega'}. \quad (11)$$



The projected Green's functions  $G_{f,b}$  are obtained by taking the limit  $\lambda \rightarrow \infty$  as discussed above. As a consequence, the energy eigenvalues of  $H + \lambda Q$  are shifted by  $\lambda Q$ . It is useful to shift the zero of the frequency scale by  $\lambda$  (in the  $Q = 1$  sector) and to define the projected spectral functions as

$$\mathcal{A}_{f,b}(\omega) = \lim_{\lambda \rightarrow \infty} A_{f,b}(\omega + \lambda) \quad (12)$$

At zero temperature the  $\mathcal{A}_{f,b}(\omega)$  have the Lehmann representation

$$\mathcal{A}_f(\omega) = \sum_n |\langle 1, n | f_\sigma^\dagger | 0, 0 \rangle|^2 \delta(\omega + E_0^0 - E_n^1) \quad (13)$$

and correspondingly for  $\mathcal{A}_b$ , where  $E_n^0$  are the energy eigenvalues ( $E_0^0$  is the ground state energy) and  $|Q, n\rangle$  the many-body eigenstates of  $H$  in the sector  $Q$  of Fock space. The  $\mathcal{A}_{f,b}$  show threshold behavior at  $\omega = E_0 \equiv E_0^1 - E_0^0$ , with  $\mathcal{A}_{f,b}(\omega) \equiv 0$  for  $\omega < 0$ . The vanishing imaginary part at frequencies  $\omega < 0$  may be shown to be a general property of all quantities involving slave particle operators, e.g. also of auxiliary particle selfenergies and vertex functions.

Both  $\mathcal{A}_f(\omega)$  and  $\mathcal{A}_b(\omega)$  are found to diverge for  $\omega \rightarrow E_0$  in a power law fashion (infrared singularity)

$$\mathcal{A}_{f,b} \sim |\omega - E_0|^{-\alpha_{f,b}} \theta(\omega - E_0) \quad (14)$$

due to a diverging number of particle-hole excitation processes in the conduction electron sea for  $\omega \rightarrow E_0$ .

For the single channel case ( $M = 1$ ), i.e. the usual Kondo or mixed valence problem, the exponents  $\alpha_f$  and  $\alpha_b$  can be found analytically from the following argumentation. Anticipating that in this case the impurity spin is completely screened by the conduction electrons at temperature  $T = 0$ , leaving a pure-potential scattering center, the ground state  $|1, 0\rangle$  is a Slater determinant of one particle scattering states, characterized by scattering phase shifts  $\eta_\sigma^0$  in the s-wave channel (assuming for simplicity a momentum independent hybridization matrix element  $V$ ). The scattering phase shifts are related to the fraction of conduction electrons attracted (or repelled) by the impurity,  $\Delta n_\sigma$ , via the Friedel sum rule as  $\eta_\sigma^0 = \pi \Delta n_\sigma$ . The change in the average number of conduction electrons per scattering channel  $\sigma$  due to the presence of the impurity exactly matches the average occupation number of the impurity level per spin channel,  $\Delta n_\sigma = -n_d/N$ , where  $n_d$  is the total occupation of the impurity level. In the Kondo limit  $n_d \rightarrow 1$  and for a spin 1/2 impurity this leads to resonance scattering,  $\eta_\sigma^0 = \pi/2$ . To calculate now the spectral function  $\mathcal{A}_f(\omega)$  from Eq. (13), one needs to evaluate  $\langle 1, n | f_\sigma^\dagger | 0, 0 \rangle$ , which

is nothing but the overlap of two Slater determinants, the ground state of the conduction electron system in the absence of the impurity combined with the decoupled impurity level occupied by an electron with spin  $\sigma$ ,  $f_\sigma^\dagger|0,0\rangle$ , on the one hand, and the eigenstates of the fully interacting Kondo system,  $|1,n\rangle$ , on the other hand. As shown by Anderson<sup>24</sup>, the overlap of the two ground state Slater determinants  $\langle 1,0 | f_\sigma^\dagger | 0,0\rangle$  tends to zero in the thermodynamic limit (orthogonality catastrophe). This implies that the spectral functions diverge at the threshold as

$$A_{f\sigma}(\omega) = c |\omega|^{-\alpha_f} \quad (15)$$

where  $\alpha_f = 1 - \sum_{\sigma'} (\eta_{\sigma'}/\pi)^2$ . Here the  $\eta_{\sigma'}$  are the scattering phase shifts relative to the state  $f_\sigma^\dagger | 0,0\rangle$ . Using again the Friedel sum rule one finds  $\eta_{\sigma'} = \pi n_d/N$  for  $\sigma' \neq \sigma$ . In the scattering channel  $\sigma$  the change in the number of conduction electrons is  $\Delta n_\sigma = n_d/N - 1$ , since the occupation in the initial state  $n_{d\sigma}^{in} = 1$  is reduced by interaction processes to  $n_{d\sigma} = n_d/N$  in the final state. As a result, one finds<sup>25</sup> the exponent  $\alpha_f = (2n_d - n_d^2)/N$ . A similar consideration for the slave boson spectral function yields  $\alpha_b = 1 - n_d^2/N$ . These results have been found independently from Wilson's numerical renormalization group approach<sup>26</sup> and using the Bethe ansatz solution and boundary conformal field theory<sup>27</sup>. It is interesting to note that (i) the exponents depend on the level occupancy  $n_d$  (in the Kondo limit  $n_d \rightarrow 1$ ,  $\alpha_f = 1/N$  and  $\alpha_b = 1 - 1/N$ , whereas in the opposite, empty orbital, limit  $n_d \rightarrow 0$ ,  $\alpha_f \rightarrow 0$  and  $\alpha_b \rightarrow 1$ ) (ii) the sum of the exponents  $\alpha_f + \alpha_b = 1 + 2\frac{n_d(1-n_d)}{N} \geq 1$ .

We stress that the above derivation of the infrared exponents  $\alpha_{f,b}$  holds true only if the impurity complex acts as a pure potential scattering center at  $T = 0$ . This is equivalent to the statement that the conduction electrons behave locally, i.e. at the impurity site, like a Fermi liquid. Conversely, in the multi-channel (non-FL) case,  $N \geq 2$ ,  $M \geq N$ , the exponents have been found from a conformal field theory solution<sup>21</sup> of the problem in the Kondo limit to be  $\alpha_f = M/(M+N)$ ,  $\alpha_b = N/(M+N)$ , which differ from the FL values. Thus, one may infer from the values of  $\alpha_{f,b}$  as a function of  $n_d$ , whether or not the system is in a local Fermi liquid state.

The physical electron Green's functions for the local d-electrons and for the conduction electrons  $\mathcal{G}_d(i\omega_n)$  and  $\mathcal{G}_c(\vec{k}, \vec{k}'; i\omega_n)$ , can be expressed through the self-energy  $\Sigma_c(i\omega_n)$  as<sup>28</sup>

$$\mathcal{G}_d(i\omega_n) = \frac{1}{V^2} \lim_{\lambda \rightarrow \infty} e^{\beta\lambda} \Sigma_c(i\omega_n) \quad (16)$$

and

$$\mathcal{G}_c(\vec{k}, \vec{k}'; i\omega_n) = G_c^0(\vec{k}, i\omega_n) \left[ \delta_{\vec{k}, \vec{k}'} + V^2 \mathcal{G}_d(i\omega_n) G_c^0(\vec{k}', i\omega_n) \right] \quad (17)$$

## 4 Mean field and non-crossing approximations

For physical situations of interest, the  $s - d$  hybridization of the Anderson model (1) is much smaller than the conduction band width,  $N_0V \ll 1$ , where  $N_o = 1/2D$  is the local conduction electron density of states at the Fermi level. This suggests a perturbation expansion in  $N_oV$ . A straightforward expansion in terms of bare Green's functions is not adequate, as it would not allow to capture the physics of the Kondo screened state, or else the infrared divergencies of the auxiliary particle spectral functions discussed in the last section. In the framework of the slave boson representation, two types of nonperturbative approaches have been developed. The first one is mean field theory for both the slave boson amplitude  $\langle b \rangle$  and the constraint ( $\langle Q \rangle = 1$  rather than  $Q = 1$ ). The second one is resummation of the perturbation theory to infinite order.

### 4.1 Slave boson mean field theory

Slave boson mean field theory is based on the assumption that the slave bosons condense at low temperatures such that  $\langle b_\mu \rangle \neq 0$ . Replacing the operator  $b_\mu$  in  $H + \lambda Q$  by  $\langle b_\mu \rangle$  (see Ref. [22]), where  $\lambda$  is a Lagrange multiplier to be adjusted such that  $\langle Q \rangle = 1$ , one arrives at a resonance level model for the pseudofermions. The position of the resonance,  $E_d + \lambda$ , is found to be given by the Kondo temperature  $T_K$ , and is thus close to the Fermi energy. The resonance generates the low energy scale  $T_K$ , and leads to local Fermi liquid behavior. While this is qualitatively correct in the single-channel case, it is in blatant disagreement with the exactly known behavior in the multi-channel case. The mean field theory can be shown to be exact for  $M = 1$  in the limit  $N \rightarrow \infty$  for a model in which the constraint is softened to be  $Q = N/2$ . However, for finite  $N$  it is known that the fluctuations in the phase of the complex expectation value  $\langle b_\mu \rangle$  are divergent and lead to the suppression of  $\langle b_\mu \rangle$  to zero. This is true in the cartesian gauge, whereas in the radial gauge the phase fluctuations may be shown to cancel at least in lowest order. It has not been possible to connect the mean field solution, an apparently reasonable description at low temperatures and for  $M = 1$ , to the high temperature behavior ( $T \gg T_K$ ), dominated by logarithmic temperature dependence, in a continuous way<sup>29</sup>. Therefore, it seems that the slave boson mean field solution does not offer a good starting point even for only a qualitatively correct description of quantum impurity models.

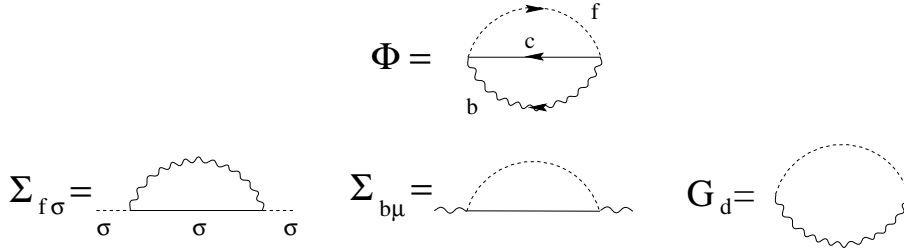


Figure 2: Diagrammatic representation of the generating functional  $\Phi$  of the NCA. Also shown are the pseudoparticle selfenergies and the local electron Green's function derived from  $\Phi$ , Eqs. (19)–(21). Throughout this article, dashed, wavy and solid lines represent fermion, boson, and conduction electron lines, respectively. In the diagram for  $\Sigma_{f\sigma}$  the spin labels are shown explicitly to demonstrate that there are no coherent spin fluctuations taken into account.

#### 4.2 $1/N$ expansion vs. self-consistent formulation

The critical judgement of mean field theory is corroborated by the results of a straightforward  $1/N$ -expansion in the single channel case, keeping the exact constraint, and not allowing for a finite bose field expectation value<sup>30</sup>. Within this scheme the exact behavior of the thermodynamic quantities (known from the Bethe ansatz solution) at low temperatures as well as high temperatures is recovered to the considered order in  $1/N$ . Also, the exact auxiliary particle exponents  $\alpha_{f,b}$  are reproduced in order  $1/N$ , using a plausible exponentiation scheme<sup>31</sup>.

In addition, dynamical quantities like the d-electron spectral function and transport coefficients can be calculated exactly to a desired order in  $1/N$ , within this approach. However, as clear-cut and economical this method may be, it does have serious limitations. For once, the experimentally most relevant case of  $N = 2$  or somewhat larger is not accessible in  $1/N$  expansion. Secondly, non-Fermi liquid behavior, being necessarily non-perturbative in  $1/N$ , cannot be dealt with in a controlled way on the basis of a  $1/N$ -expansion. To access these latter two regimes, a new approach nonperturbative in  $1/N$  is necessary.

We conjecture that this new approach is gauge invariant many-body theory of pseudofermions and slave bosons. As long as gauge symmetry violating objects such as Bose field expectation values or fermion pair correlation functions do not appear in the theory, gauge invariance of physical quantities can be guaranteed in suitably chosen approximations by the proper match of pseudofermion and slave boson properties, without introducing an additional gauge field. This requires the use of conserving approximations<sup>32</sup>, derived from a

Luttinger-Ward functional  $\Phi$ .  $\Phi$  consists of all vacuum skeleton diagrams built out of fully renormalized Green's functions  $G_{b,f,c}$  and the bare vertex  $V$ . The self-energies  $\Sigma_{b,f,c}$  are obtained by taking the functional derivative of  $\Phi$  with respect to the corresponding Green's function (cutting the Green's function line in each diagram in all possible ways),

$$\Sigma_{b,f,c} = \delta\Phi/\delta G_{b,f,c}. \quad (18)$$

Irreducible vertex functions, figuring as integral kernels in two-particle Bethe-Salpeter equations, are generated by second order derivatives of  $\Phi$ .

The choice of diagrams for  $\Phi$  defines a given approximation. It should be dictated by the dominant physical processes and by expansion in a small parameter, if available. As noted before, in the present context, we may take the hybridization  $V$  to be a small quantity (dimensionless parameter  $N_oV$ ). This suggests to start with the lowest order (in  $V$ ) diagram of  $\Phi$ , which is second order (see Fig. 2). The self-energies generated from this obey after projection the following equations of self-consistent second order perturbation theory<sup>28</sup>

$$\Sigma_{f\sigma}(\omega - i0) = V^2 \sum_{\mu} \int d\varepsilon [1 - f(\varepsilon)] A_{c\mu\sigma}^0(\varepsilon) G_{b\mu}(\omega - \varepsilon - i0) \quad (19)$$

$$\Sigma_{b\mu}(\omega - i0) = V^2 \sum_{\sigma} \int d\varepsilon f(\varepsilon) G_{f\sigma}(\omega + \varepsilon - i0) A_{c\mu\sigma}^0(\varepsilon) \quad (20)$$

$$G_{d\mu\sigma}(\omega - i0) = \int d\varepsilon e^{-\beta\varepsilon} [G_{f\sigma}(\omega + \varepsilon - i0) \mathcal{A}_{b\mu}(\varepsilon) - \mathcal{A}_{f\sigma}(\varepsilon) G_{b\mu}(\varepsilon - \omega + i0)], \quad (21)$$

where  $A_{c\mu\sigma}^0 = 1/\pi \text{Im}G_{c\mu\sigma}^0$  is the (free) conduction electron density of states and  $f(\varepsilon) = 1/(\exp(-\beta\varepsilon) + 1)$  denotes the Fermi distribution function. Together with the expressions (9), (10) for the Green's functions, Eqs. (19)–(21) form a set of self-consistent equations for  $\Sigma_{b,f,c}$ , comprised of all diagrams without any crossing propagator lines and, thus, known as the “non-crossing approximation”, in short NCA.

At zero temperature and for low frequencies Eqs. (19) and (20) may be converted into a set of linear differential equations for  $G_f$  and  $G_b$ <sup>33</sup>, which allow to find the infrared exponents as  $\alpha_f = \frac{M}{M+N}$ ;  $\alpha_b = \frac{N}{M+N}$ , independent of  $n_d$ . For the single channel case these exponents do not agree with the exact exponents derived in section 3. This indicates that the NCA is not capable of recovering the local Fermi liquid behavior for  $M = 1$ . A numerical evaluation of the  $d$ -electron Green's function, which is given by the local self-energy  $\Sigma_c$

divided by  $V^2$  and hence is given by the boson-fermion bubble within NCA (Fig. 2), shows indeed a spurious singularity at the Fermi energy<sup>28</sup>. The NCA performs somewhat better in the multi-channel case, where the exponents  $\alpha_f$  and  $\alpha_b$  yield the correct non-Fermi liquid exponents of physical quantities as known from the Bethe ansatz solution<sup>20</sup> and conformal field theory<sup>21</sup>. However, the specific heat and the residual entropy are not given correctly in NCA. Also, the limiting low temperature scaling laws for the thermodynamic quantities are attained only at temperatures substantially below  $T_K$ , in disagreement with the exact Bethe ansatz solution.

## 5 Conserving T-matrix approximation

In order to eliminate the shortcomings of the NCA mentioned above, the guiding principle should be to find contributions to the vertex functions which renormalize the auxiliary particle threshold exponents to their correct values, since this is a necessary condition for the description of FL and non-FL behavior, as discussed in section 3. Furthermore, it is instructive to realize that in NCA any coherent spin flip and charge transfer processes are neglected, as can be seen explicitly from Eqs. (19), (20) or from Fig. 2. These processes are known to be responsible for the quantum coherent collective behavior of the Anderson impurity complex below  $T_K$ . The existence of collective excitations in general is reflected in a singular behavior of the corresponding two-particle vertex functions. In view of the tendency of Kondo systems to form a collective spin singlet state, we are here interested in the spin singlet channel of the pseudofermion-conduction electron vertex function and in the slave boson-conduction electron vertex function. It may be shown by power counting arguments that there are no corrections to the NCA exponents in any finite order of perturbation theory<sup>34</sup>. Thus, we are led to search for singularities in the aforementioned vertex functions arising from an infinite resummation of terms. From the preceding discussion it is natural to perform a partial resummation of those terms which, at each order in the hybridization  $V$ , contain the maximum number of spin flip or charge fluctuation processes, respectively. This amounts to calculating the conduction electron-pseudofermion vertex function in the “ladder” approximation defined in Fig. 3, where the irreducible vertex is given by  $V^2 G_b$ . In analogy to similar resummations for an interacting one-component Fermi system, we call the total c-f vertex function T-matrix  $T^{(cf)}$ . The Bethe-Salpeter equation for  $T^{(cf)}$  reads (Fig. 3),

$$T_{\sigma\sigma',\sigma'}^{(cf)}(i\omega_n, i\omega'_n, i\Omega) = - V^2 G_b(i\omega_n + i\omega'_n - i\Omega) \delta_{\sigma\sigma'} \delta_{s'\sigma}$$

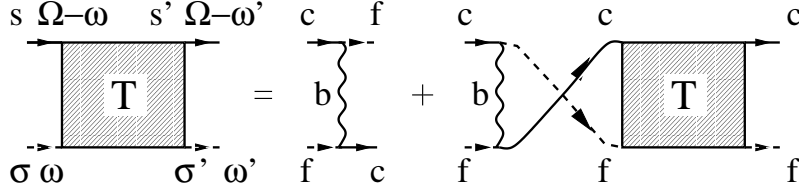


Figure 3: Diagrammatic representation of the Bethe-Salpeter equation for the conduction electron-pseudofermion T-matrix  $T^{(cf)}$ , Eq. (22). The conduction electron-slave boson T-matrix  $T^{(cb)}$  is obtained by interchanging  $f \leftrightarrow b^\dagger$ .

$$\begin{aligned}
 & + V^2 T \sum_{\omega''_n} G_b(i\omega_n + i\omega''_n - i\Omega) \times \\
 & G_{f\sigma}(i\omega''_n) G_{cs}(-i\omega''_n + i\Omega) T_{\sigma s, s' \sigma'}^{(cf)}(i\omega''_n, i\omega'_n, i\Omega).
 \end{aligned} \tag{22}$$

A similar integral equation holds for the charge fluctuation T-matrix  $T^{(cb)}$ . Inserting NCA Green's functions for the intermediate state propagators of Eq. (22) and solving it numerically, we find at low temperatures and in the Kondo regime ( $n_d \gtrsim 0.7$ ) a pole of  $T^{(cf)}$  in the singlet channel as a function of the center-of-mass (COM) frequency  $\Omega$ , at a frequency which scales with the Kondo temperature,  $\Omega = \Omega_{cf} \simeq -T_K$ . This is shown in Fig. 4. The threshold behavior of the imaginary part of  $T^{(cf)}$  as a function of  $\Omega$  with vanishing spectral weight at negative frequencies and temperature  $T = 0$  is clearly seen. In addition, a very sharp structure appears, whose broadening is found to vanish as the temperature tends to zero, indicative of a pole in  $T^{(cf)}$  at the *real* frequency  $\Omega_{cf}$ , i.e. the tendency to form a collective singlet state between the conduction electrons and the localized spin. Similarly, the corresponding T-matrix  $T^{(cb)}$  in the conduction electron-slave boson channel, evaluated within the analogous approximation, develops a pole at negative values of  $\Omega$  in the empty orbital regime ( $n_d \lesssim 0.3$ ). In the mixed valence regime ( $n_d \simeq 0.5$ ) the poles in both  $T^{(cf)}$  and  $T^{(cb)}$  coexist. The appearance of poles in the two-particle vertex functions  $T^{(cf)}$  and  $T^{(cb)}$ , which signals the formation of collective states, may be expected to influence the behavior of the system in a major way.

On the level of approximation considered so far, the description is not yet consistent: In the limit of zero temperature the spectral weight of  $T^{(cf)}$  and  $T^{(cb)}$  at negative frequencies  $\Omega$  should be strictly zero (threshold property). Nonvanishing spectral weight at  $\Omega < 0$  like a pole contribution for negative  $\Omega$  in  $T^{(cf)}$  or  $T^{(cb)}$  would lead to a diverging contribution to the self-energy, which is unphysical. However, recall that a minimum requirement on the ap-

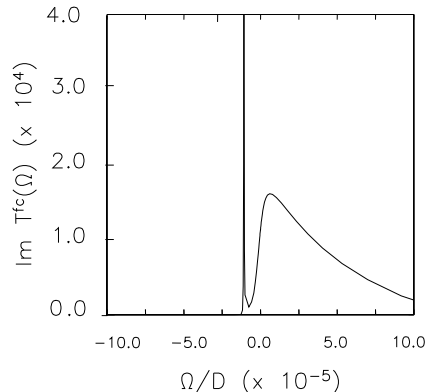


Figure 4: Imaginary part of the conduction electron–pseudofermion T–matrix  $T^{(cf)}$  as a function of the COM frequency  $\Omega$  for the single–channel case  $M = 1$ ,  $N = 2$ , evaluated by inserting NCA solutions for the intermediate state propagators ( $E_d = -0.67D$ ,  $\Gamma = 0.15D$ ,  $T = 4 \cdot 10^{-3}T_K$ ). The contribution from the pole positioned at a negative frequency  $\Omega = \Omega_{cf} \simeq -T_K$  (compare text) is clearly seen.

proximation used is the conservation of gauge symmetry. This requirement is not met when the integral kernel of the  $T$ -matrix equation is approximated by the NCA result. Rather, the approximation should be generated from a Luttinger–Ward functional. The corresponding generating functional is shown in Fig. 5. It is defined as the infinite series of all vacuum skeleton diagrams which consist of a single ring of auxiliary particle propagators, where each conduction electron line spans at most two hybridization vertices. The first diagram of this series corresponds to NCA (Fig. 2). The diagram containing two boson lines is excluded since it is not a skeleton. Although the spirit of the present theory is different from a large  $N$  expansion, it should be noted that the sum of the  $\Phi$  diagrams containing up to four boson lines includes all terms of a  $1/N$  expansion up to  $O(1/N^2)$ <sup>35</sup>. By functional differentiation with respect to the conduction electron Green’s function and the pseudofermion or the slave boson propagator, respectively, the shown  $\Phi$  functional generates the ladder approximations  $T^{(cf)}$ ,  $T^{(cb)}$  for the total conduction electron–pseudofermion vertex function (Fig. 3) and for the total conduction electron–slave boson vertex function. The auxiliary particle self–energies are obtained in the conserving scheme as the functional derivatives of  $\Phi$  with respect to  $G_f$  or  $G_b$ , respectively (Eq. (18)). This defines a set of self–consistency equations, which we term conserving T–matrix approximation (CTMA), where the self-energies are given as nonlinear and nonlocal (in time) functionals of the Green’s functions, while



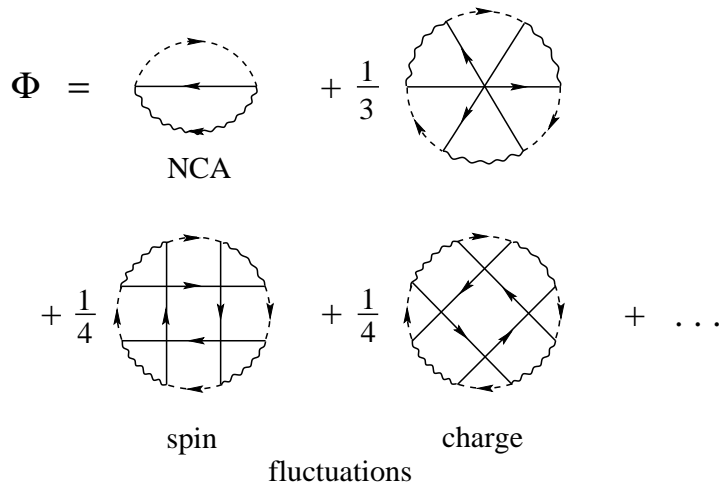


Figure 5: Diagrammatic representation of the Luttinger–Ward functional generating the conserving T–matrix approximation (CTMA). The terms with the conduction electron lines running clockwise (labelled “spin fluctuations”) generate the T–matrix  $T^{(cf)}$ , while the terms with the conduction electron lines running counter–clockwise (labelled “charge fluctuations”) generate the T–matrix  $T^{(cb)}$ .

the Green’s functions are in turn expressed in terms of the self–energies. The solution of these equations requires that the T–matrices have vanishing spectral weight at negative COM frequencies  $\Omega$ . Indeed, the numerical evaluation shows that the poles of  $T^{(cf)}$  and  $T^{(cb)}$  are shifted to  $\Omega = 0$  by self–consistency, where they merge with the continuous spectral weight present for  $\Omega > 0$ , thus renormalizing the threshold exponents of the auxiliary spectral functions.

The self-consistent solutions are obtained by first solving the linear Bethe–Salpeter equations for the T–matrices by matrix inversion, computing the auxiliary particle self–energies from  $T^{(cf)}$  and  $T^{(cb)}$ , and then constructing the fermion and boson Green’s functions from the respective self–energies. This process is iterated until convergence is reached. We have obtained reliable solutions down to temperatures of the order of at least  $10^{-2}T_K$  both for the single-channel and for the two-channel Anderson model. Note that  $T_K \rightarrow 0$  in the Kondo limit; in the mixed valence and empty impurity regimes, significantly lower temperatures may be reached, compared to the low temperature scale of the model.

As shown in Fig. 6 (1) a), the auxiliary particle spectral functions obtained from CTMA<sup>36</sup> are in good agreement with the results of a numerical renor-

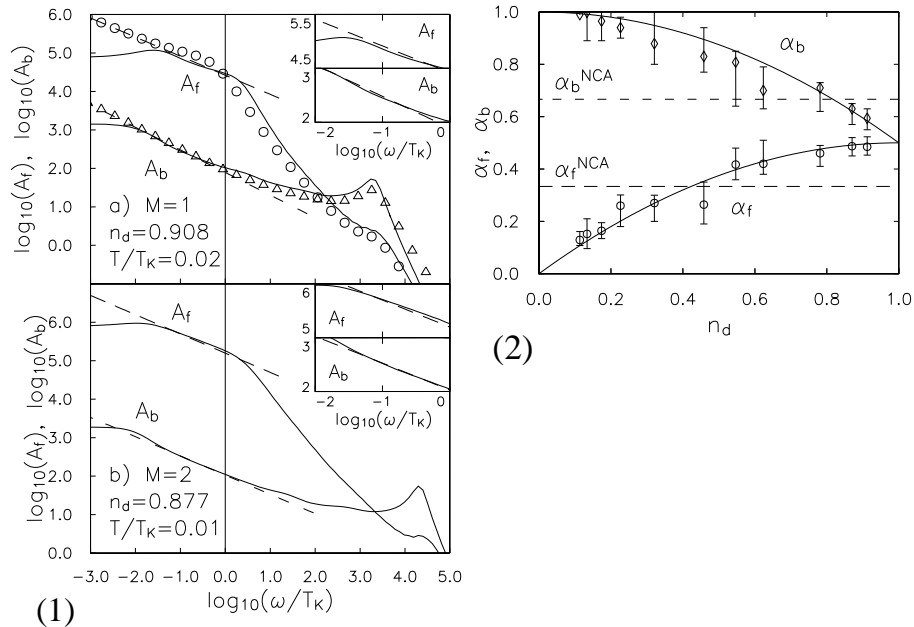


Figure 6: (1) Pseudofermion and slave boson spectral functions  $A_f$  and  $A_b$  in the Kondo regime ( $N = 2$ ;  $E_d = -0.05$ ,  $\Gamma = 0.01$  in units of the half-bandwidth  $D$ ), for a) the single-channel ( $M = 1$ ) and b) the multi-channel ( $M = 2$ ) case. In a) the symbols represent the results of NRG for the same parameter set,  $T = 0$ . The slopes of the dashed lines indicate the exact threshold exponents as derived in section 3 for  $M = 1$  and as given by conformal field theory for  $M = 2$ . The insets show magnified power law regions. (2) CTMA results (symbols with error bars) for the threshold exponents  $\alpha_f$  and  $\alpha_b$  of  $A_f$  and  $A_b$ ,  $N = 2$ ,  $M = 1$ . Solid lines: exact values (section 3), dashed lines: NCA results (section 4.2).

malization group (NRG) calculation<sup>26</sup> (zero temperature results), given the uncertainties in the NRG at higher frequencies. Typical behavior in the Kondo regime is recovered: a broadened peak in  $A_b$  at  $\omega \simeq |E_d|$ , representing the hybridizing  $d$ -level and a structure in  $A_f$  at  $\omega \simeq T_K$ . Both functions display power law behavior at frequencies below  $T_K$ , which at finite  $T$  is cut off at the scale  $\omega \simeq T$ . The exponents extracted from the frequency range  $T < \omega < T_K$  of our finite  $T$  results compare well with the exact result also shown (see insets of Fig. 6 (1a)). A similar analysis has been performed for a number of parameter sets spanning the complete range of  $d$ -level occupation numbers  $n_d$ . The extracted power law exponents are shown in Fig. 6 (2), together with error bars estimated from the finite frequency ranges over which the fit was made.

The comparatively large error bars in the mixed valence regime arise because here spin flip and charge fluctuation processes, described by the poles in  $T^{(cf)}$  and  $T^{(cb)}$ , respectively, are of equal importance, impeding the convergence of the numerical procedure. In this light, the agreement with the exact results (solid curves) is very good, the exact value lying within the error bars or very close in each case.

In the multi-channel case ( $N \geq 2, M \geq N$ ) NCA has been shown<sup>34</sup> to reproduce asymptotically the correct threshold exponents,  $\alpha_f = M/(M+N)$ ,  $\alpha_b = N/(M+N)$ , in the Kondo limit. Calculating the T-matrices using NCA Green's functions (as discussed in the single-channel case) we find again a pole in the singlet channel of  $T^{(cf)}$ . However, the weight of the pole vanishes in the Kondo limit  $n_d \rightarrow 1$ . As a result, the CTMA does not renormalize the NCA exponents in the Kondo limit of the two-channel model, i.e. the threshold exponents obtained from the CTMA solutions are very close to the exact ones,  $\alpha_f = 1/2, \alpha_b = 1/2$ , as shown in Fig. 6 (1) b).

The agreement of the CTMA exponents with their exact values in the Kondo, mixed valence and empty impurity regimes of the single-channel model and in the Kondo regime of the two-channel model may be taken as evidence that the T-matrix approximation correctly describes both the FL and the non-FL regimes of the  $SU(N) \times SU(M)$  Anderson model ( $N=2, M=1,2$ ). Therefore, we expect the CTMA to correctly describe physically observable quantities of the  $SU(N) \times SU(M)$  Anderson impurity model as well. In Fig. 7 we show the static spin susceptibility  $\chi$  of the two-channel Anderson model in the Kondo regime. It is seen that CTMA correctly reproduces the exact<sup>20</sup> logarithmic temperature dependence below the Kondo scale  $T_K$ . In contrast, the NCA solution recovers the logarithmic behavior only far below  $T_K$ . Other physical quantities will be calculated for the Anderson model in forthcoming work.

## 6 Conclusion

We have presented a novel technique to describe correlated quantum impurity systems with strong onsite repulsion, which is based on a gauge invariant formulation of the auxiliary boson method. This technique allows for the first time to describe physical quantities, like the magnetic susceptibility, over the complete temperature range, including the crossover to the correlated many-body state at the lowest temperatures. The numerical effort involved in the evaluations of the multiple integrals is manageable, considering that one complete iteration within the self-consistent scheme has been done on a parallel computer within approximately 5–10 s CPU time. As a standard diagram technique this method has the potential to be applicable to problems of cor-

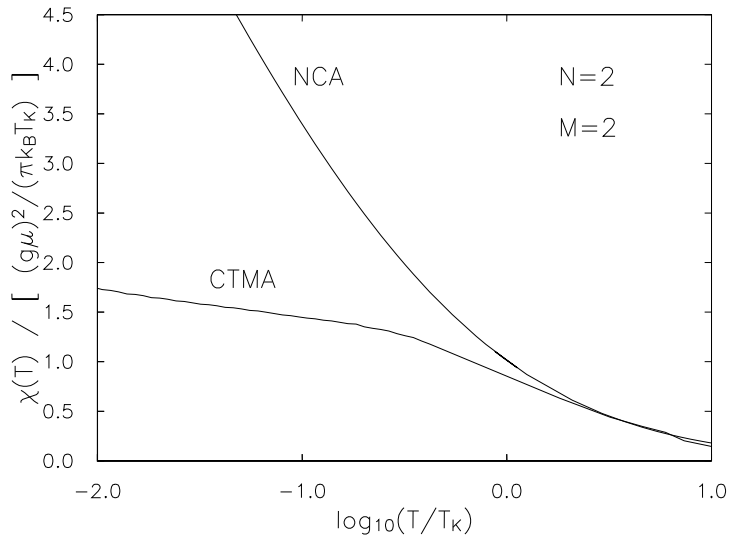


Figure 7: Static susceptibility of the two-channel Anderson impurity model: CTMA and NCA results ( $E_d = -0.8D$ ,  $\Gamma = 0.1D$ , Landé factor  $g = 2$ ).

related systems on a lattice as well, while keeping the full dynamics of the pseudofermion and slave boson fields.

We wish to thank S. Böcker, T.A. Costi, A. Rosch, and A. Ruckenstein for stimulating discussions. S. Böcker has performed part of the numerical solutions. This work is supported by DFG through SFB 195 and by the Hochleistungsrechenzentrum Jülich through a grant of computer time on a Cray T3E parallel computer.

## References

1. L.D. Landau, Sov.Phys. JETP **3**, 920 (1956); **5**, 101 (1957); **8**, 70 (1959).
2. H. v. Loehneysen et al., Phys. Rev. Lett. **72**, 3262 (1994); B. Bogenberger and H. v. Loehneysen, Phys. Rev. Lett. **74**, 1016 (1995).
3. H. v. Loehneysen, J. Phys. Cond. Mat. **8** 9689 (1996).
4. F. Steglich, J. Phys. Cond. Mat. **8** 9909 (1996).
5. F. M. Grosche, S. R. Julian, N. D. Mathur and G. G. Lonzarich, Physica B **223** + **224**, 50 (1996).
6. S. R. Julian et al., J. Phys. Cond. Mat. **8** 9675 (1996).
7. M. B. Maple et al., J. Low Temp. Phys. **95**, 225 (1994); **99**, 223 (1995);

- M. B. Maple et al., J. Phys. Cond. Mat. **8** 9773 (1996).
8. R. Chain and M. B. Maple, J. Phys. Cond. Mat. **8** 9939 (1996).
  9. A. J. Millis, Phys. Rev. B **48**, 7183 (1993).
  10. T. Moriya and T. Takimoto, J. Phys. Soc. Japan **64**, 960 (1995)
  11. A. Rosch et al., Phys. Rev. Lett. **79**, 159 (1997).
  12. For non-FL behavior near a quantum spin-glass transition, see S. Sachdev, N. Read and R. Oppermann, Phys. Rev. B **52**, 10286 (1995).
  13. P. Nozierès and A. Blandin, J. Phys. (Paris) **41**, 193 (1980).
  14. A comprehensive overview appears in D. L. Cox and F. Zawadowski, Adv. Phys. in press (1998); (cond-mat/9704103).
  15. D.L. Cox, Phys. Rev. Lett. **59**, 1240 (1987); Physica C 153, 1642 (1988).
  16. J.R. Schrieffer and P.A. Wolff, Phys. Rev. **B149**, 491 (1966).
  17. K. G. Wilson, Rev. Mod. Phys. **47**, 773 (1975).
  18. N. Andrei, K. Furuya, J.H. Löwenstein, Rev.Mod.Phys. **55**, 331 (1983).
  19. A. M. Tsvelik, J. Phys. C **18** 159 (1985).
  20. P.B. Wiegmann, A.M. Tsvelik, Pis'ma Zh. Eksp. Teor. Fiz. **38**, 489 (1983) [JETP Lett. **38**, 591 (1983)]; N. Andrei, C. Destri, Phys. Rev. Lett. **52**, 364, (1984).
  21. I. Affleck and A.W.W. Ludwig, Nucl. Phys. **352**, 849, (1991); **B360**, 641, (1991); Phys. Rev. B **48**, 7297 (1993).
  22. S. E. Barnes, J. Phys. **F6**, 1375 (1976); **F7**, 2637 (1977).
  23. A. A. Abrikosov, Physics **2**, 21 (1965).
  24. P. W. Anderson, Phys. Rev. Lett. **18**, 1049 (1967).
  25. B. Menge and E. Müller-Hartmann, Z. Phys. **B73**, 225 (1988).
  26. T.A. Costi, P. Schmitteckert, J. Kroha and P. Wölfle, Phys. Rev. Lett. **73**, 1275 (1994).
  27. S. Fujimoto, N. Kawakami and S.K. Yang, J.Phys.Korea **29**, S136 (1996).
  28. For details of the derivation and evaluation at low temperatures see T.A. Costi, J. Kroha, and P. Wölfle, PRB **53**, 1850 (1996).
  29. D. M. Newns and N. Read, Adv. Phys. **36**, 799 (1988).
  30. B. Jin and Y. Kuroda, J. Phys. Soc. Japan **57**, 1687 (1988).
  31. T. Matsuura et al., J. Phys. Soc. Japan **66**, 1245 (1997).
  32. G. Baym and L.P. Kadanoff, Phys. Rev. **124**, 287 (1961); G. Baym, Phys. Rev. **127** 1391 (1962).
  33. E. Müller-Hartmann, Z. Phys. **B57**, 281 (1984).
  34. D. L. Cox and A. E. Ruckenstein, Phys. Rev. Lett. **71**, 1613 (1993).
  35. F. Anders and N. Grewe, Europhys. Lett. **26**, 551 (1994); F. Anders, J. Phys. Cond. Mat. **7**, 2801 (1995).
  36. J. Kroha, P. Wölfle and T. A. Costi, Phys. Rev. Lett. **79**, 261 (1997).